# An Experimental and Numerical Investigation of Distortion and Residual Stress in GTAW Dissimilar Pipe Welds

**Hamdani**
School of Engineering, Universitas Syiah Kuala, Banda Aceh, Indonesia | Department of Mechanical Engineering, Politeknik Negeri Lhokseumawe, Lhokseumawe, Indonesia
hamdani_jtm@pnl.ac.id

**Akhyar Akhyar**
Department of Mechanical Engineering, Universitas Syiah Kuala, Banda Aceh, Indonesia
akhyar@usk.ac.id (corresponding author)

**Thaib Rizwan**
Department of Capture Fisheries, Marine and Fisheries Faculty, Universitas Syiah Kuala, Banda Aceh, Indonesia
rizwanthaib@usk.ac.id

**Agus Sasmito**
Research Center for Hydrodynamic Technology, National Research and Innovation Agency of Indonesia, Surabaya, Indonesia
agus.sasmito@brin.go.id

*Received: 26 March 2026 | Revised: 3 May 2026 | Accepted: 8 May 2026*

 *DOI: https://doi.org/10.48084/etasr.18937*

**ABSTRACT**

**Welding dissimilar metals often results in complex thermo-mechanical behavior due to differences in material properties, which can lead to distortion and residual stress. This study evaluates the thermo-mechanical response of SUS304–SA213-T11 dissimilar pipe welds using a coupled numerical–experimental methodology. Gas Tungsten Arc Welding (GTAW) was performed with varying heat inputs, and a sequentially coupled finite element model was developed to predict temperature distribution, distortion, and residual stress. A dial gauge and the magnetic-based Stress Vision technique were used to take experimental measurements of deformation and residual stress. The findings indicate that with increasing welding current, the peak temperature and Heat Affected Zone (HAZ) area increase. Both deformation and residual stress decrease with increased current due to less heat accumulation caused by high travel speed. The highest deformation and residual stress occurred at 70 A, and the lowest at 90 A. The results stand as evidence that heat accumulation is the driving factor for the thermo-mechanical behavior of dissimilar pipe welds instead of current, thus elaborating a valuable insight to enhance welding parameters in industries.**

***Keywords-dissimilar welding; residual stress; distortion; FEA; pipe welding***

## I. INTRODUCTION

Dissimilar Metal Welding (DMW) is commonly used in engineering systems where components with different properties must be joined, particularly in piping systems in the energy and process industries. A common combination is austenitic stainless steel (SUS304) and low-alloy steel (SA213-T11), which provides good mechanical strength and economic advantages [1-3]. These materials are widely used in industrial piping systems, particularly in power generation and petrochemical applications, where components must withstand high temperatures, pressures, and corrosive environments, improving performance and durability under arduous service conditions. However, DMW results in new thermo-mechanical behavior due to the dissimilar thermal and mechanical properties of the bonded materials. The thermal conductivity and coefficients of thermal expansion differ, resulting in non-uniform heating and cooling that leads to residual stresses and

distortion due to welding [4, 5]. These effects are more apparent in pipe structures because they must maintain dimensional stability and structural integrity under pressure and cyclic loading conditions [6, 7]. The temperature distribution, residual stress evolution, and deformation during welding have been predicted using Finite Element Analysis (FEA) [8, 9]. Authors in [5, 7, 10] conducted experimental investigations in order to evaluate distortion and confirm numerical predictions. Authors in [11, 12] focused on plate geometries or separated direct numerical analysis on the interaction between thermal loads, residual stress, and pipe deformation in circumferential welds. Furthermore, some methods of measuring residual stress are destructive or semi-destructive, which restricts their usage on actual structures. Authors in [13, 14] proposed magnetic-based non-destructive methods as an alternative to represent stress situations in ferromagnetic materials and characterize stress concentration rapidly and non-invasively. Authors in [15-18] demonstrated that welding parameters, particularly heat input and welding sequence, significantly impact residual stress and distortion in pipe welding. DMW presents challenges, including brittle intermetallic formation, carbon migration, and steep thermal gradients, all of which generate residual stress. These factors reduce joint integrity and long-term reliability, especially under high-temperature and high-pressure conditions. Differences in physical and metallurgical properties further complicate weld behavior, increasing distortion and cracking. Therefore, controlling heat input and welding parameters is significant because these factors strongly influence weld performance and require an integrated thermo-mechanical analysis [19-21]. This study investigates the thermo-mechanical behavior of SUS304–SA213-T11 dissimilar pipe joints using a combined numerical-experimental approach that integrates FEA, distortion measurement, and magnetic-based residual stress mapping.

## II. MATERIALS AND METHODS

### A. Materials and Welding Procedure

Table I presents the chemical compositions of the base materials and filler metal, while Table II summarizes their mechanical properties.

TABLE I. CHEMICAL COMPOSITION OF MATERIALS AND FILLER METAL (WT.%)

| Materials | C | Mn | Si | Cr | Ni | Mo | S | P | Cu |
|---|---|---|---|---|---|---|---|---|---|
| SUS304 | 0.08 | 2.00 | 1.00 | 18 – 20 | 8 – 10.5 | - | 0.03 | 0.045 | - |
| SA213-T11 | 0.05 – 0.15 | 0.3 – 0.6 | 0.5 – 1.00 | 1 – 1.5 | - | 0.44 – 0.65 | 0.025 max | 0.025 max | - |
| ER308 | 0.03 | 1 – 2.5 | 0.3 – 0.65 | 19.5 – 22 | 9 – 11 | 0.75 max | 0.03 max | 0.03 max | 0.75 max |

TABLE II. MECHANICAL PROPERTIES OF MATERIALS AND FILLER METAL

| Material | Min. yield strength (MPa) | Min. tensile strength (MPa) | Elastic modulus (GPa) | Hardness rockwell |
|---|---|---|---|---|
| SUS304 | 290 | 579 | 200 | B80 |
| SA213-T11 | 205 | 415 | 215 | B85 |
| ER308 | 400 | 580 | 200 | B89 |

The DMW configuration is shown in Figure 1. Butt-joint pipe specimens with a diameter of 44.5 mm, a length of 100 mm, and a thickness of 4 mm were welded using GTAW with ER308 filler metal. A single V-groove with a 70° angle, a 3-mm root gap, and a 1.5-mm root face was used, as depicted in Figure 1 (a). Welding was performed in the 5G position with DCEN polarity and a constant voltage of 18 V, as portrayed in Figure 1 (b). To vary heat input, welding currents of 70 A, 80 A, and 90 A were applied with travel speeds of 2 mm/s, 3 mm/s, and 4 mm/s. The interphase temperature was kept at 300°C with internal argon purging to prevent oxidation and ensure weld quality [22]. The groove geometry, filler metal, and welding parameters were selected based on industrial standards and prior research to ensure weld quality and consistency. ER308 filler was chosen because of its compatibility with austenitic stainless steel and to reduce the risk of cracking. Preliminary trials were performed to determine the welding parameters (70–90 A, 18 V, and 2–4 mm/s), which were chosen to maintain a controlled heat input and a stable arc. Variations in current and travel speed were applied to evaluate the effect of heat accumulation on thermo-mechanical behavior. High-purity argon shielding and internal purging were used to maintain weld quality and prevent oxidation. Visual inspection and non-destructive ultrasonic testing confirmed the absence of surface defects. The agreement between the experimental and numerical results indicates the reliability and integrity of the welded joints.

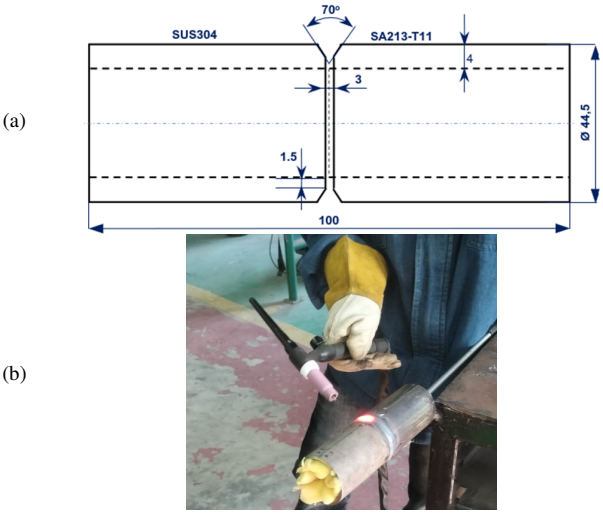


Fig. 1. Welding set-up: (a) butt-joint design, (b) welding process.

### B. Deformation and Residual Stress Measurement

Deformation due to welding and residual stress was assessed using an experimental approach, as illustrated in Figure 2. Radial deformation was measured with a dial gauge, whereas distortion was measured at predetermined circumferential positions. Pipe diameters were compared before and after welding to quantify out-of-roundness [6, 21]. Residual stress distribution was evaluated using a Stress Vision

system based on the Indicator of Mechanical Stress (IMS) principle. This nondestructive method uses the magnetoelastic effect to identify zones of stress concentration and principal stress gradients. Although it is qualitative, this method effectively maps residual stress distribution in welded components [13, 14].

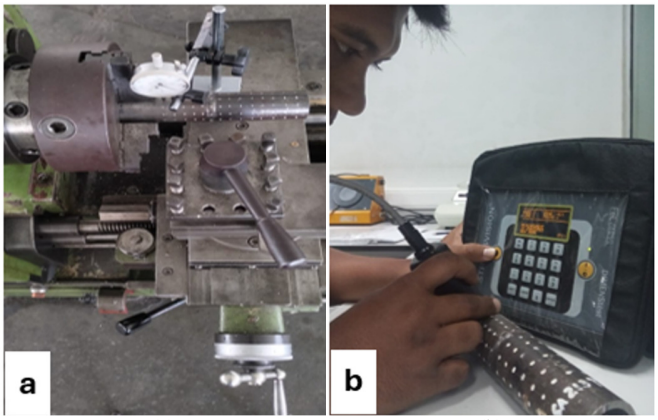


(a) (b)

Fig. 2. Experiment set-up for: (a) deformation measurement, (b) residual stress measurement.

### C. Finite Element Analysis

A sequentially coupled thermo-mechanical analysis was performed, using ANSYS Workbench, starting with a transient thermal analysis, and then a structural analysis to predict deformation and residual stress [22, 23]. ANSYS ACT was used to implement a moving heat source along the circumferential welding path around the pipe. The heat source was modeled using a Gaussian surface heat flux distribution:

$$q(r) = q_0 \exp\left(-\frac{3r^2}{R^2}\right) \quad (1)$$

where $q_0$ is the peak heat flux and $R$ is the effective heat source radius. Heat input was defined as:

$$Q = \eta \frac{VI}{v} \quad (2)$$

The heat input was calculated using the following values: $\eta$ = 0.7–0.8, $V$ = 18 V, $I$ = 70–90 A, and $v$ = 2–4 mm/s. A heat flux of 12–16 W/mm² with a radius of 5 mm was calibrated to produce a realistic temperature distribution and weld pool behavior. The model was validated through the strong correlation between the simulation and experimental results, particularly regarding the trends in deformation and residual stress. Convective heat loss (25 W/m²·K) and room-temperature initial conditions were considered. The structural model employed thermoelastic-plastic behavior with temperature-dependent von Mises plasticity. A refined mesh with partial constraints was applied in the weld and Heat Affected Zone (HAZ), as exhibited in Figure 3. The mesh was refined in the weld and HAZ to capture steep thermal gradients and stress concentrations. While a full mesh sensitivity analysis was not conducted, the mesh was sufficient, as confirmed by result convergence and good agreement with experimental observations. The thermal results were mapped into the structural analysis, and the model was validated based on experimental measurements.

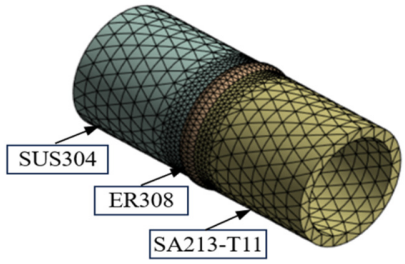


Fig. 3. FEA model and mesh generation.

## III. RESULTS AND DISCUSSION

### A. Thermal Behavior and Temperature Distribution

Figure 4 shows the temperature distribution.

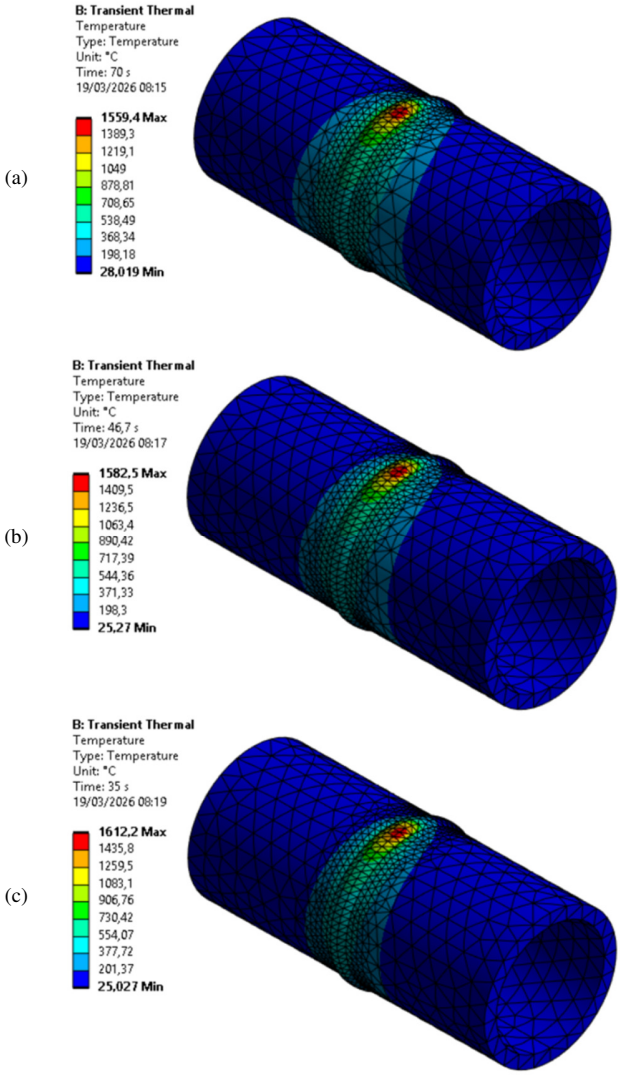


Fig. 4. Temperature distribution during welding at: (a) 70 A, (b) 80 A, and (c) 90 A.

The peak temperature is concentrated along the circumferential weld path, which indicates effective localization of the heat source. As the welding current increases from 70 A to 90 A, both the maximum temperature and the size of the HAZ increase. At 70 A, the thermal field is relatively confined, resulting in a narrow HAZ. Conversely, a wider spread of heat is observed for higher currents (80 A and 90 A) due to the high input power. This behavior reflects the direct relationship between heat input and arc energy in the welding process. Thus, larger heat input increases the peak temperature and strengthens thermal accumulation.

### *B. Welding-Induced Deformation*

Figure 5 presents the deformation modes from the simulated process.

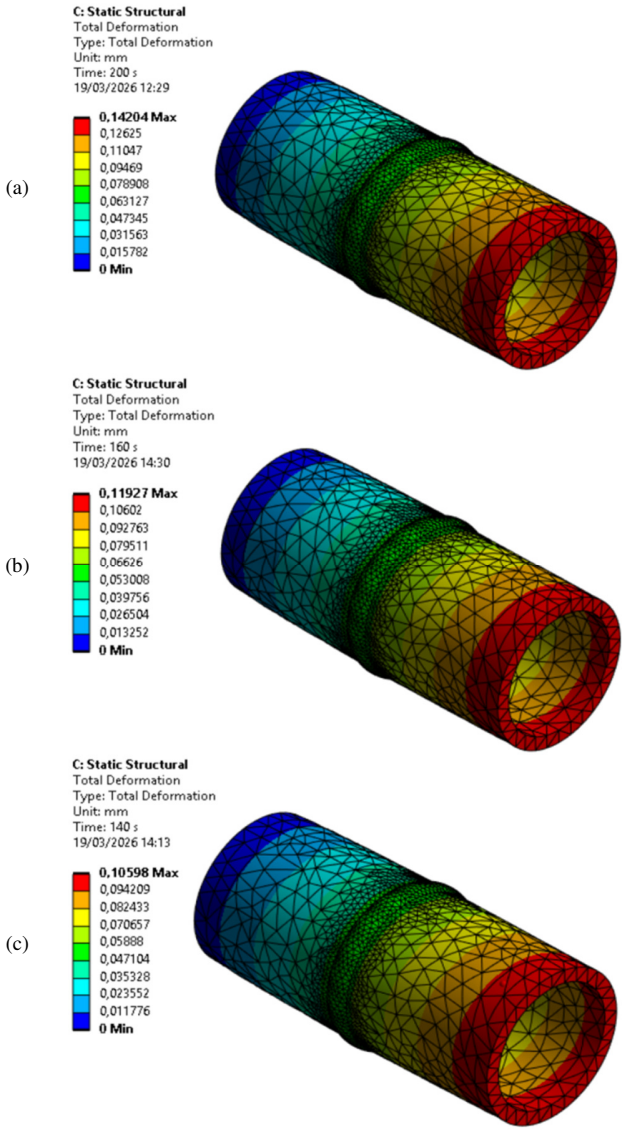


Fig. 5. The deformation pattern for: (a) 70 A, (b) 80 A, and (c) 90 A.

Deformation is localized within the weld region and propagates along the pipe's axis, suggesting non-uniform thermal expansion and contraction. The maximum deformation was less at higher welding currents. Maximum deformation occurs at 70 A (approximately 0.142 mm), followed by 80 A (approximately 0.119 mm), whereas minimum deformation occurs at 90 A (approximately 0.106 mm). At a travel speed of 70 A, the material is exposed to heat for a longer time, resulting in more thermal accumulation and distortion [24]. This indicates that heat input and thermal cycle duration govern deformation behavior. Lower currents and speeds increase heat accumulation and distortion, whereas higher currents and faster travel speeds reduce it. Additionally, thermal property mismatch intensifies localized deformation at the weld interface. Figure 6 demonstrates that the highest deformation decreases as the welding electric current rises. Although higher current generates more heat per unit of time, higher travel speeds mean that the amount of accumulated heat per unit length decreases. This results in less dramatic thermal contraction, contributing to less distortion at higher current levels.

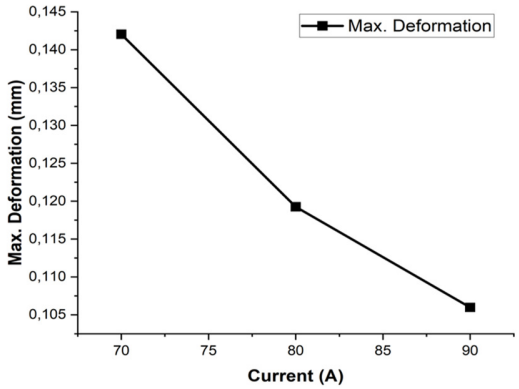


Fig. 6. Relationship between welding current and maximum deformation.

### *C. Deformation Validation*

The validation of the deformation is presented in Figure 7. The numerical models show the observed distortion pattern at both ends of the pipe. The ~0.1% discrepancy may be attributed to experimental uncertainty and the assumptions made during numerical modeling. Nevertheless, the model correctly predicts the overall deformation trend.

### *D. Residual Stress Distribution and Validation*

Figure 8 displays the residual stress distribution. At higher currents, the maximum stress decreases from approximately 432 MPa at 70 A to approximately 322 MPa at 80 A and 263 MPa at 90 A. This is because shorter thermal cycles allow for less heat accumulation and, consequently, lower stresses. In every case, the localized weld and the dissimilar interface are associated with stress. Figure 8 provides a comparison of the simulation results (left) and Stress Vision measurements (right). Both approaches show a strong concentration of stresses in the weld region. Thus, this agreement indicates that the model accurately captures the distribution of residual stress. Authors in [25, 26] showed that thermal gradients and heat accumulation were identified as the dominant factors influencing stress distribution in welded structures.

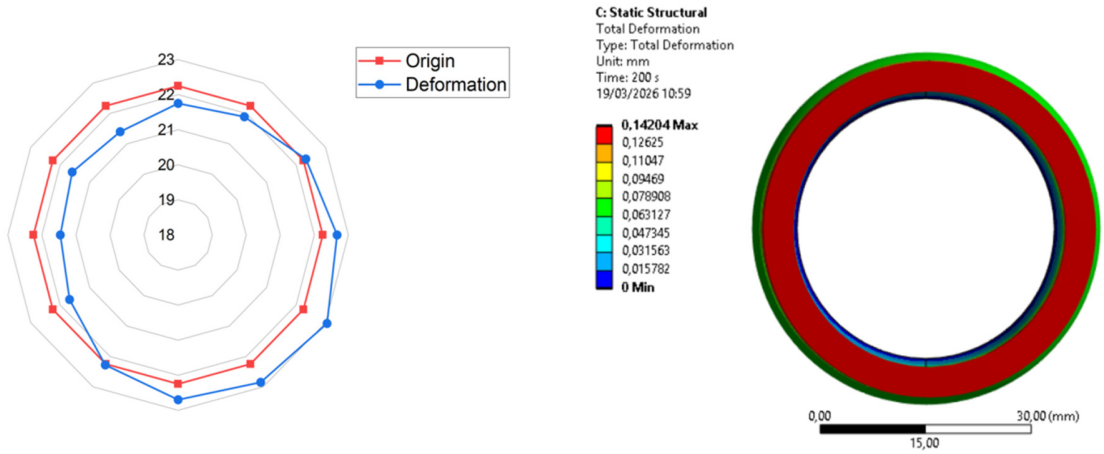


(a)

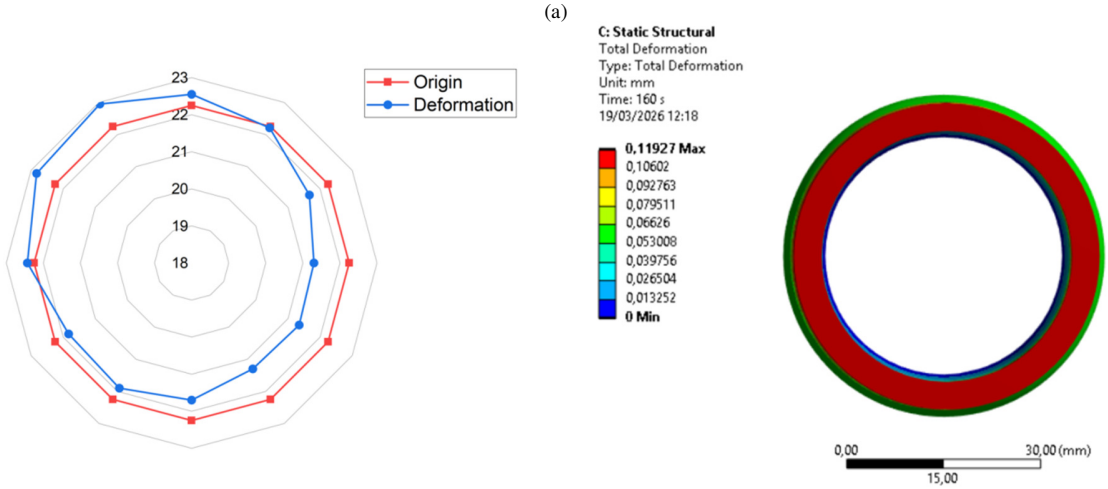


(b)

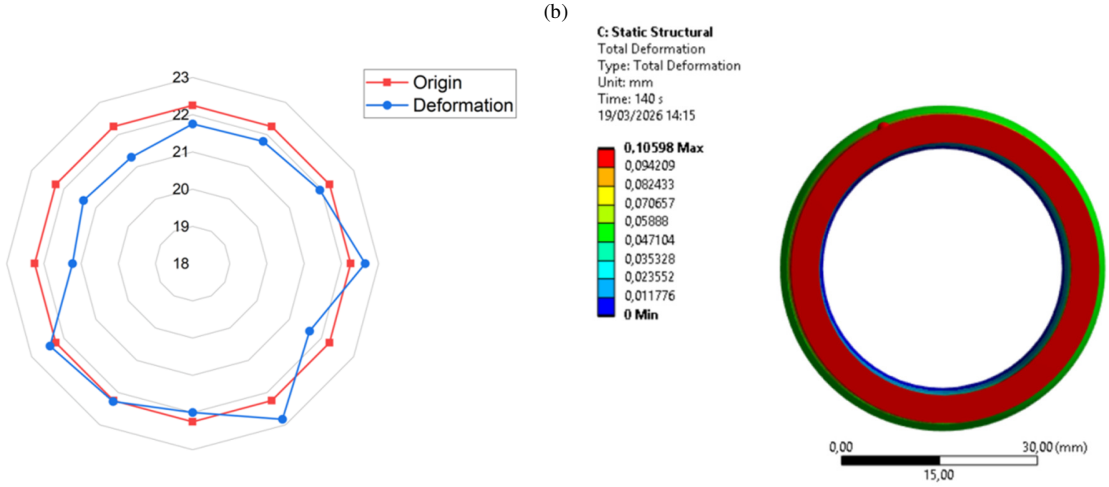


(c)

Fig. 7. Validation of deformation behavior for: (a) 70 A, (b) 80 A, and (c) 90 A.

### *E. Effect of Heat Input on Thermo-Mechanical Response*

The heat input significantly influences the overall thermo-mechanical behavior of the welded joint. A higher welding current results in a higher temperature, a broader HAZ, a more extensive residual stress distribution, and greater deformation. Of the tested conditions, 80 A produces a balanced response with moderate deformation and a fairly even stress distribution. Conversely, 70 A produces inadequate thermal penetration. At a higher current of 90 A, increased travel speed reduces heat accumulation per unit length despite the higher instantaneous heat input, resulting in lower overall distortion. These results demonstrate the necessity of controlling heat input to ensure weld quality and establish a balance between providing

adequate mechanical strength and transporting pipes. An increase in the interpass temperature to 300°C influences the thermal cycle and residual stress evolution. Maintaining an elevated interpass temperature minimizes thermal gradients between successive weld passes and the surrounding material, reducing abrupt cooling and stress concentration. These conditions create a more uniform temperature distribution and reduce residual stress intensity. Although Stress Vision measurements show good agreement with numerical results regarding stress distribution patterns, this technique provides qualitative rather than quantitative values. Therefore, the focus of the comparison is on the consistency of stress localization and distribution trends rather than exact magnitudes. Some uncertainty arises from the method itself and from assumptions in the numerical model.

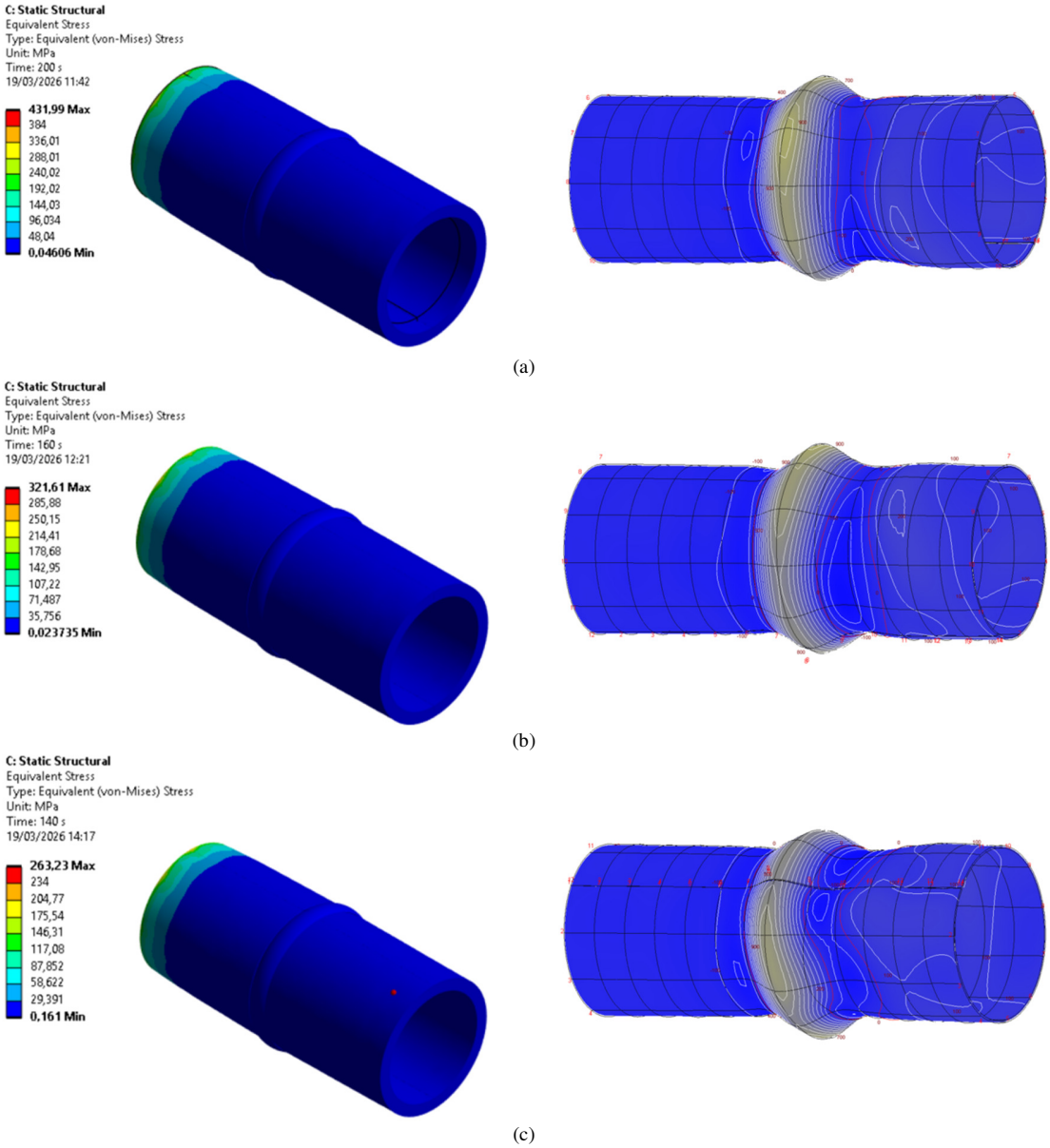


Fig. 8. Validation of residual stress for: (a) 70 A, (b) 80 A, and (c) 90 A.

The observed relationship between welding current and thermo-mechanical response is not solely governed by current magnitude, but also by its interaction with travel speed. The latter directly influences heat accumulation per unit length. While higher current increases instantaneous heat input, the corresponding increase in travel speed reduces heat exposure duration, limiting thermal diffusion and accumulation. This combined effect results in lower residual stress and deformation at higher current levels. Therefore, the present study emphasizes that heat accumulation, rather than welding current alone, dominates the thermo-mechanical behavior of dissimilar pipe welds. This finding underscores the crucial role

of heat accumulation per unit length in governing the thermo-mechanical response of dissimilar pipe welds, optimizing welding parameters.

## IV. CONCLUSIONS

The present study used a combined numerical-experimental approach to investigate the thermo-mechanical behavior of dissimilar pipe welds based on SUS304-SA213-T11. The results show that heat input plays an important role in temperature distribution, residual stress, and deformation. As the welding current increases, the peak temperature and the heat-affected zone both increase. However, deformation and residual stress decrease with increasing current due to less heat accumulation resulting from a higher travel speed. Maximum deformation and residual stress were the highest at 70 A and the lowest at 90 A, suggesting that heat accumulation rather than current controls the thermo-mechanical response. Residual stress is primarily found in the weld region and the dissimilar interface, demonstrating the effect of material mismatch on residual stress. The numerical outcomes were compared with the experimental results, indicating close agreement for both deformation and residual stress distribution, which suggests that the developed model is reliable. This study emphasizes the importance of optimizing heat input for planarity and controlling final residual stress. The combined approach used in this study provides a practical framework for selecting welding parameters in dissimilar pipe welding applications. This study contributes novel findings by combining numerical simulations, experimental deformation measurements, and magnetic-based residual stress evaluations to investigate circumferential dissimilar pipe welds. The results provide practical guidance for optimizing welding parameters in industrial piping systems, particularly for joints made of dissimilar materials that operate under high-temperature and high-pressure conditions. The study identifies heat accumulation, rather than welding current alone, as the primary parameter influencing thermo-mechanical behavior, offering a more reliable basis for parameter optimization in such applications.

## DECLARATION OF COMPETING INTERESTS

The authors have no known competing financial or personal interests that could have appeared to influence the work reported in this paper.

## ACKNOWLEDGMENT

This publication was made possible by a grant from the Ministry of Higher Education, Science, and Technology of the Republic of Indonesia.

## DATA AVAILABILITY

The data used and analyzed during the current study are available from the corresponding author upon reasonable request.

## AI USE AND DECLARATION OF GENERATIVE AI USE

No sections of the text, figures, or experimental results were generated using artificial intelligence tools.

## REFERENCES

[1] H. Eisazadeh and D. K. Aidun, "Residual stress reduction in dissimilar metals weld," *Journal of Manufacturing Processes*, vol. 64, pp. 1462–1475, 2021, https://doi.org/10.1016/j.jmapro.2021.02.062.

[2] S. Zhang *et al*., "Experimental characterisation and numerical modelling of residual stresses in a nuclear safe-end dissimilar metal weld joint," *Metals*, vol. 11, no. 8, 2021, Art. no. 1298, https://doi.org/10.3390/met11081298.

[3] H. Hamdani, A. Akhyar, T. Rizwan, A. Sasmito, and H. A. Suhartono, "Mechanical and metallurgical properties of GTAW dissimilar welds between SUS304 and SA213T11 using ER308 filler metal, preliminary study," *Advances in Science and Technology Research Journal*, vol. 19, no. 8, pp. 77–89, 2025, https://doi.org/10.12913/22998624/204768.

[4] C. L. Tsai and D. S. Kim, "Understanding residual stress and distortion in welds: An overview," in *Processes and Mechanisms of Welding Residual Stress and Distortion*, 2005, pp. 3–31, https://doi.org/10.1533/9781845690939.1.3.

[5] S. Das Banik, S. Kumar, P. K. Singh, S. Bhattacharya, and M. M. Mahapatra, "Distortion and residual stresses in thick plate weld joint of austenitic stainless steel: Experiments and analysis," *Journal of Materials Processing Technology*, vol. 289, 2021, Art. no. 116944, https://doi.org/10.1016/j.jmatprotec.2020.116944.

[6] P. C. Adamczuk, I. G. Machado, and J. A. E. Mazzaferro, "Methodology for predicting the angular distortion in multi-pass butt-joint welding," *Journal of Materials Processing Technology*, vol. 240, pp. 305–313, 2017, https://doi.org/10.1016/j.jmatprotec.2016.10.006.

[7] M. Zubairuddin, S. K. Albert, S. Mahadevan, M. Vasudevan, V. Chaudhari, and V. K. Suri, "Experimental and finite element analysis of residual stress and distortion in GTA welding of modified 9Cr-1Mo steel," *Journal of Mechanical Science and Technology*, vol. 28, no. 12, pp. 5095–5105, 2014, https://doi.org/10.1007/s12206-014-1132-0.

[8] P. Jhunjhunwala, P. Taraphdar, A. Gupta, and C. Pandey, "Numerical simulation of temperature fields and residual stresses in multi-pass weld using the novel prescribed temperature approach with experimental validation," *Transactions of the Indian Institute of Metals*, vol. 75, no. 10, pp. 2713–2723, 2022, https://doi.org/10.1007/s12666-022-02625-2.

[9] R. Kumar, A. K. Pradhan, M. M. Mahapatra, P. K. Taraphdar, C. Pandey, and K. Sridhar, "Exploring through-thickness residual stress distribution in double V-groove multipass welds of high-strength low-alloy steel and the impact of mechanical restraints," *Journal of Materials Engineering and Performance*, vol. 34, no. 15, pp. 16768–16779, 2025, https://doi.org/10.1007/s11665-024-10357-1.

[10] H. R. Raftar, A. Ahola, K. Lipiäinen, and T. Björk, "Simulation and experiment on residual stress and deflection of cruciform welded joints," *Journal of Constructional Steel Research*, vol. 208, 2023, Art. no. 108023, https://doi.org/10.1016/j.jcsr.2023.108023.

[11] Y. Liu, P. Wang, H. Fang, and N. Ma, "Characteristics of welding distortion and residual stresses in thin-walled pipes by solid-shell hybrid modelling and experimental verification," *Journal of Manufacturing Processes*, vol. 69, pp. 532–544, 2021, https://doi.org/10.1016/j.jmapro.2021.08.014.

[12] C. Wu and J.-W. Kim, "Analysis of welding residual stress formation behavior during circumferential TIG welding of a pipe," *Thin-Walled Structures*, vol. 132, pp. 421–430, 2018, https://doi.org/10.1016/j.tws.2018.09.020.

[13] L. Y. Mogilner, V. A. Syasko, and A. I. Shikhov, "Modeling defects in ultrasonic nondestructive testing: State-of-the-art and prospects," *Russian Journal of Nondestructive Testing*, vol. 60, no. 5, pp. 481–500, 2024, https://doi.org/10.1134/S1061830924700657.

[14] W. Akhtar, I. Lazoglu, and S. Y. Liang, "Prediction and control of residual stress-based distortions in the machining of aerospace parts: A review," *Journal of Manufacturing Processes*, vol. 76, pp. 106–122, 2022, https://doi.org/10.1016/j.jmapro.2022.02.005.

[15] I. Sattari-Far and Y. Javadi, "Influence of welding sequence on welding distortions in pipes," *International Journal of Pressure Vessels and Piping*, vol. 85, no. 4, pp. 265–274, 2008, https://doi.org/10.1016/j.ijpvp.2007.07.003.

[16] D. Deng, S. Kiyoshima, K. Ogawa, N. Yanagida, and K. Saito, "Predicting welding residual stresses in a dissimilar metal girth welded pipe using 3D finite element model with a simplified heat source," *Nuclear Engineering and Design*, vol. 241, no. 1, pp. 46–54, 2011, https://doi.org/10.1016/j.nucengdes.2010.11.010.

[17] C. H. Lee and K. H. Chang, "Effect of the welding sequence in the circumferential direction on residual stress distribution in a thin-walled pipe weld," *Proceedings of the Institution of Mechanical Engineers, Part B: Journal of Engineering Manufacture*, vol. 223, no. 6, pp. 723–735, 2009, https://doi.org/10.1243/09544054JEM1362.

[18] N. Moslemi *et al*., "Influence of welding sequences on induced residual stress and distortion in pipes," *Construction and Building Materials*, vol. 342, 2022, Art. no. 127995, https://doi.org/10.1016/j.conbuildmat.2022.127995.

[19] V. Bhanu, A. Gupta, and C. Pandey, "Role of A-TIG process in joining of martensitic and austenitic steels for ultra-supercritical power plants: A state of the art review," *Nuclear Engineering and Technology*, vol. 54, no. 8, pp. 2755–2770, 2022, https://doi.org/10.1016/j.net.2022.03.003.

[20] N. Kumar, P. Kumar, D. Fydrych, and C. Pandey, "Dissimilar gas metal arc welding (GMAW) of Inconel 718 and 304L stainless steel: a comparative study of ERNiCrCoMo-1 and ERNiCr-3 filler metals," *International Journal of Pressure Vessels and Piping*, vol. 220, Apr. 2026, Art. no. 105732, https://doi.org/10.1016/j.ijpvp.2025.105732.

[21] A. Garga, A. Verma, S. Kumar, V. Badheka, Hirshikesh, and C. Pandey, "Pulsed GMAW induced microstructural refinement and mechanical performance of dissimilar AISI 304H-Inconel 617 welds," *Materials Today Communications*, vol. 52, Mar. 2026, Art. no. 115006, https://doi.org/10.1016/j.mtcomm.2026.115006.

[22] S. Kou, *Welding Metallurgy*, 2nd ed. Hoboken, NJ, USA: John Wiley & Sons, 2003.

[23] D. Deng and H. Murakawa, "Numerical simulation of temperature field and residual stress in multi-pass welds in stainless steel pipe and comparison with experimental measurements," *Computational Materials Science*, vol. 37, no. 3, pp. 269–277, 2006, https://doi.org/10.1016/j.commatsci.2005.07.007.

[24] Y. P. Yang, "Recent advances in the prediction of weld residual stress and distortion—Part 2," *Welding Journal*, vol. 100, no. 6, pp. 193S–206S, 2021, https://doi.org/10.29391/2021.100.016.

[25] S. Kumar, S. M. Pandey, S. Sirohi, D. Fydrych, and C. Pandey, "P92 steel and Inconel 617 alloy welds joint produced using ERNiCr-3 filler with GTAW process: Solidification mechanism, microstructure, mechanical properties and residual stresses," *Heliyon*, vol. 9, no. 8, 2023, Art. no. e18959, https://doi.org/10.1016/j.heliyon.2023.e18959.

[26] A. K. Maurya, W. N. Khan, A. Patnaik, S. M. Pandey, R. Chhibber, and C. Pandey, "Tribological behavior and residual stresses of gas tungsten arc welded dissimilar joint of sDSS 2507/X-70 pipeline steel," *Metallurgical and Materials Transactions B*, vol. 55, no. 3, pp. 1619–1634, 2024, https://doi.org/10.1007/s11663-024-03053-x.